

Thermodynamic and Kinetic Studies for Adsorption of Reactive Blue (RB-19) Dye Using Calix[4]arene-Based Adsorbent

Ranjhan Junejo,[†] Shahabuddin Memon,[†] Fakhar N. Memon,[‡] Ayaz Ali Memon,^{*,†} Fatih Durmaz,[§] Asif Ali Bhatti,^{||} and Ashfaque Ali Bhatti[†]

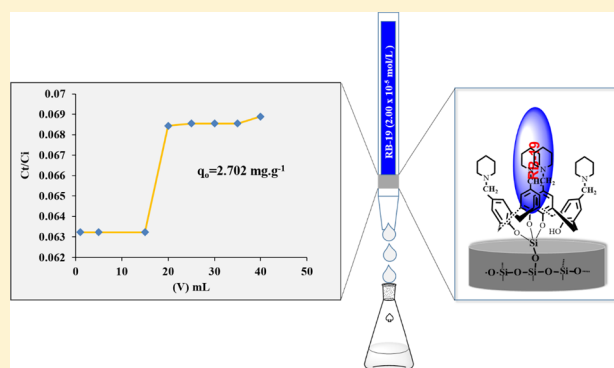
[†]National Center of Excellence in Analytical Chemistry, University of Sindh, Jamshoro 76080, Pakistan

[‡]Department of Chemistry, University of Karachi, Karachi 75270, Pakistan

[§]Department of Chemistry, Selcuk University, Konya 42075, Turkey

^{||}Department of Chemistry, Government College University Hyderabad, Hyderabad 71000, Pakistan

ABSTRACT: A current study demonstrates the removal of Reactive Blue 19 (RB-19) from industrial wastewater by synthesizing *p*-piperdinocalix[4]arene-immobilized silica resin (PASR). The surface morphology and functional group analysis were performed with scanning electron microscopy and Fourier transform infrared spectroscopy. The dye removal efficiency of PASR was analyzed through adsorption studies. Different parameters were optimized such as the pH value of dye, amount of resin, concentration of dye, and effect of electrolyte on adsorption. The adsorption mechanism was analyzed with Langmuir, Freundlich, and Dubinin–Radushkevich (D–R) isotherms. It was found that experimental data follow the Freundlich isotherm, which suggests multilayer adsorption. The column adsorption study was also evaluated by breakthrough and Thomas models. The Thomas model rate constant k_{TH} ($\text{cm}^3 \text{mg}^{-1} \text{min}^{-1}$) and maximum solid phase concentration was found to be $q_0 = 2.702 \text{ mg}\cdot\text{g}^{-1}$. The thermodynamic study reveals that the adsorption process is exothermic and spontaneous in nature. The kinetic study suggests that the adsorption process follows the pseudo-second-order kinetic model.



1. INTRODUCTION

Synthetic colorants such as azo dyes are used in industries worldwide.^{1,2} It is reported that about 7×10^5 tons of dyes are produced each year and used in the textile, food, and ink production.^{3,4} The textile industry is a major cause of water pollution because of the dye effluent.^{5,6} About 1000 tons of the textile waste effluent has been discharged each year into fresh water, which contains a number of different unreacted azo dyes.^{7,8} Reactive dyes are anionic dyes that can be easily dissolved in water and mainly used for dyeing of cotton rayon, silk, wool, nylon, etc.^{9,10} The chemical structure of the dye molecule is biologically inactive, but degradation by microorganisms makes it possible to cleave the azo ($\text{N}=\text{N}$) group, which results in the formation of aromatic amines that are toxic as well as carcinogenic in nature.^{11,12} Thus, they become harmful for the aquatic life and cause many environmental problems.¹³ Conventionally, different techniques were used for the removal of azo dyes such as adsorption, photodegradation, membrane separation, electrolytic chemical treatment, catalytic processes, and ozone treatment.¹⁴ The adsorption process has got much more attention for the treatment of dye-contaminated water due to easy application, low cost, higher efficiency, and reproducibility.^{15–17} Therefore, different types of inexpensive, reproducible, and environmentally favorable

adsorbents have been produced. In this regard, calixarene-functionalized adsorbents with different solid supports have been efficiently used for the removal of azo dyes. The structural frame of calixarene serves as the receptor for a number of ionic and neutral guest species due to its flexible shape.¹⁸ The upper- or lower-rim calixarene molecule offers an appropriate place for introducing different functional groups that can bind with several toxic dyes,¹⁹ such as 5,11,17,23-tetrakis(*N*-piperidinomethyl)-25,26,27,28-tetrahydroxycalix[4]arene, 5,11,17,23-tetrakis(*N*'-methyl-*N*-piperazinomethyl)-25,26,27,28-tetrahydroxycalix[4]arene, and 5,11,17,23-tetrakis-[(dimethylamino)methyl]-25,26,27,28-tetrahydroxy-calix[4]arene, have been applied for the liquid–liquid extraction of sulfonated dyes such as red-2 (RR-2), acid black (AB), and (RB-19), respectively.²⁰ Keeping in view of the above performance of calixarene, in this study, we have synthesized the *p*-piperdinomethylcalix[4]arene and immobilized on the surface of silica to provide a solid support and increase its surface area for the maximum efficiency of dye removal with a regenerable property.

Received: March 12, 2019

Accepted: June 12, 2019

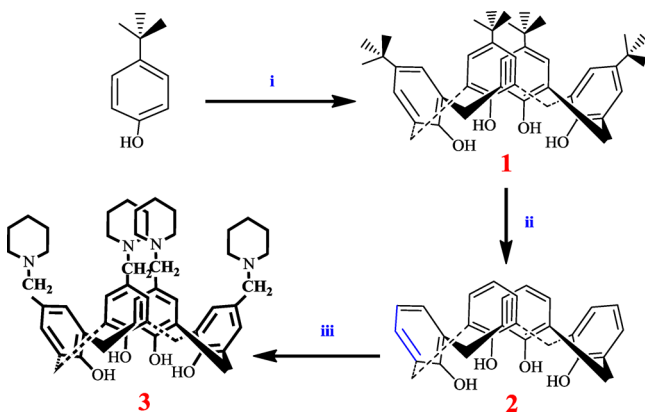
2. EXPERIMENTAL SECTION

2.1. Chemicals. All liquid reagents and solvents used during the experimental work were of analytical grade. *p*-Tertiarybutyl phenol and commercial textile RB-19 was purchased from Sigma-Aldrich (St. Louis, MO, USA). Toluene, tetrahydrofuran, dichloromethane, and chloroform were dried before use. Silica gel (130–270 particle mesh size) was purchased from Sigma-Aldrich (St. Louis, MO, USA). Precoated silica gel plates (SiO₂, Merck PF254) were used for analytical TLC. Deionized water was used for the preparation of solutions. The real wastewater samples were obtained from textile and dye industries. HCl/NaOH solutions (0.1 M) were used to maintain the pH of dye solution.

2.2. Instrumentations. FTIR spectra were recorded on a Thermo Nicolet 5700 FTIR spectrophotometer (WI. 53711, USA) as KBr pellets. A JSM-6380 instrument was used to perform scanning electron microscopy (SEM). The concentration of dye was analyzed with a Perkin Elmer (Shelton, CT06484 USA) Lambda 35 UV–VIS spectrophotometer. The pH meter (781-pH/Ion meter, Metrohm, Herisau Switzerland) with a glass electrode and an internal reference electrode was used to determine/maintain the pH values of solutions. The Gallenkamp thermostat automatic mechanical shaker (model BKS 305–101, UK) was used for the batch adsorption study.

2.3. Synthesis. Compounds **1**, **2**, and **3** were synthesized by the reported methods (Scheme 1),^{21–23} whereas the immobilization of compound **3** onto silica resin was carried out according to the following modified method.²⁴

Scheme 1. Syntheses of Calix[4]arene Derivatives: (i) HCHO/NaOH, (ii) AlCl₃/Phenol, and (iii) Piperidine/HCHO/Acetic Acid



2.3.1. Synthesis of *p*-Piperidinomethylcalix[4]arene-Immobilized Silica Resin. Five grams of silica was treated with 0.1 M HCl, filtered, and then neutralized by washing with deionized water (Scheme 2). Afterwards, the deionized silica sample was dried at about 120 °C in an oven for 8 h. Then, the dried silica sample was placed in a round-bottom flask, and 250 mL of 0.1 M SiCl₄ solution was added under stirring in CH₂Cl₂ followed by 5 mL of triethylamine and kept for 12 h at room temperature. Consequently, the solvent was removed, and 1.5 g of *p*-piperidinomethylcalix[4]arene was dissolved in chloroform that was then added in treated silica resin followed by an addition of 3 mL of trimethylamine and refluxed for 72 h. Immobilization of compound **3** was confirmed by FTIR and SEM. To remove unattached *p*-piperidinomethylcalix[4]arene

and some other possible impurities, the synthesized material was filtered and washed with 200 mL of each solvent such as CHCl₃, methanol, water, and again CHCl₃. To check the amount of attached *p*-piperidinomethylcalix[4]arene onto the silica surface, the gravimetric analysis has been performed, and it was found that the maximum amount attached onto the silica surface was 0.396 mmol/g.

2.4. Adsorption Procedure. **2.4.1. Batch Adsorption.** Batch adsorption was carried out in a 25 mL Erlenmeyer flask containing 0.075 g of adsorbent in 10 mL of RB-19 dye solution (2 × 10⁻⁵ M) and equilibrated at mechanical shaker with a constant speed of 120 rpm at 25 °C for 60 min. The adsorbent was filtered off, and the concentration of dye was analyzed before and after equilibrium by a UV–Vis spectrophotometer at λ_{max} = 596 nm. The percent (%) adsorption and adsorption capacity of RB-19 have been calculated by using the following equations:

$$\% \text{ adsorption} = \frac{C_i - C_f}{C_i} \times 100 \quad (1)$$

$$q_e = \frac{(C_i - C_e)V}{m} \quad (2)$$

2.4.2. Dynamic Adsorption Study. The dynamic adsorption study has been performed using a (6 mm × 10 cm) glass column containing the optimized quantity of the adsorbent. The dynamic adsorption capability of the adsorbent was observed by passing the solution of RB-19 dye at optimized pH with a flow rate of 2 mL/min using a peristaltic pump. The efficiency of *p*-piperidinocalix[4]arene-immobilized silica resin (PASR) was evaluated by a breakthrough curve, which gives the exhaustion capacity, and experimental data was fitted to the Thomas model to calculate the adsorption capacity.

3. RESULTS AND DISCUSSION

3.1. FTIR Analysis. The FTIR spectroscopy analysis helps to determine the presence of different functionalities in the compound. Figure 1a represents the pure silica resin spectrum that indicates a strong absorbance peak at 1094 cm⁻¹ for asymmetric Si–O–Si. The strong peak in a functional group region at 3455 cm⁻¹ appeared due to the presence of the –OH stretching band. The spectrum shown in Figure 1b shows characteristic bands for *p*-piperidinomethylcalix[4]arene (**3**), and the bands observed at 3400, 3010, 1596, and 1463 cm⁻¹ indicative of OH, CH₂, C–C, and C–N stretching, respectively. Moreover, the attachment of *p*-piperidinomethylcalix[4]arene (**3**) onto silica can be evidenced in the spectrum shown in Figure 1c. The appearance of some additional bands of *p*-piperidinomethylcalix[4]arene at 3445, 2932, 1465, and 1092 cm⁻¹ indicates the presence of OH, CH₂, C–C, and C–N of the calixarene moiety, respectively, and Si–O groups of silica confirming the immobilization of compound **3** onto the silica surface.

3.2. Scanning Electron Microscopy Analysis. Scanning electron microscopy (SEM) is the technique through which the surface morphology of the adsorbent are analyzed because the adsorption is a surface phenomenon, and the rate and degree of adsorption depend upon the surface properties that include surface area and porosity. SEM micrographs were obtained in this regard and are very demonstrative. Figure 2 shows the micrograph of pure silica. Figure 2a has smooth surface morphology; however in Figure 2b, the rough surface

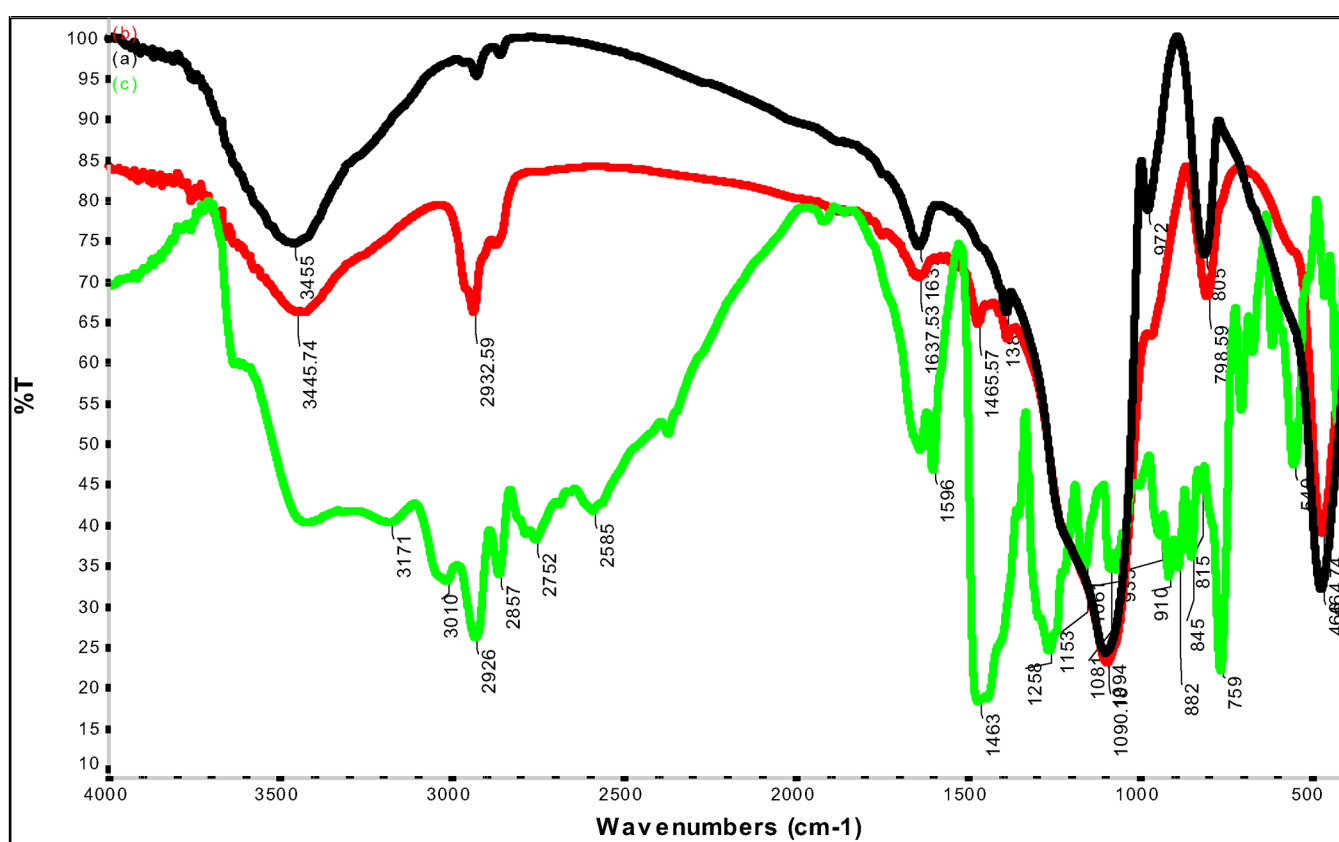
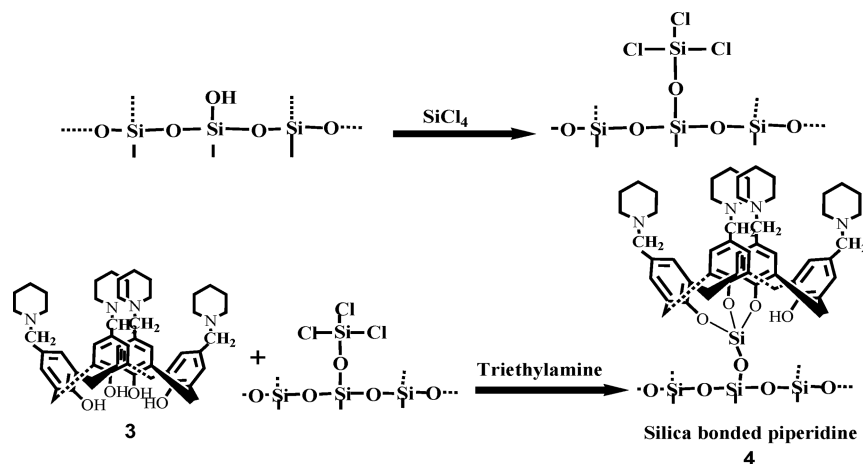
Scheme 2. Attachment of *p*-piperidinomethylcalix[4]arene onto the Silica Surface

Figure 1. FTIR spectra of (a) pure silica, (b) *p*-piperidinomethylcalix[4]aren-immobilized silica resin (PASR), and (c) *p*-piperidinomethylcalix[4]arene.

of silica can be seen due to the presence of calixarene. This irregular morphology is very helpful in the adsorption process.

3.3. Optimization of Different Parameters. **3.3.1. Dosage Effect.** The effect of the adsorbent dosage for the adsorption (RB-19) was observed by using varying amounts of adsorbent from 0.025 to 1.50 g with the fixed concentration of RB-19 (2×10^{-5} M). It can be seen from Figure 3 that the % adsorption of RB-19 increases by increasing the amount of the adsorbent. The maximum % adsorption (99% of RB-19) was observed from 0.125 g of adsorbent. After that, a very slight increase in % adsorption was detected up to 0.075 g, and it remains constant at a higher amount of the adsorbent such as

0.075–0.150 g. This may be due to the saturation of the adsorbent. Further, experiments were carried out using 0.125 g of adsorbent.

3.3.2. Electrolyte Effect. The effects of different electrolytes (NaCl, NaOH, Na_2CO_3 , CH_3COONa , and NaHCO_3) on the adsorption process have been examined. It is clear in Figure 4 that the adsorption capacity of PASR remains higher than NaCl, whereas its adsorption capability decreases with the addition of other electrolytes such as NaOH, Na_2CO_3 , CH_3COONa , and NaHCO_3 . The electrolytes affect increases in the order of $\text{NaCl} < \text{CH}_3\text{COONa} < \text{NaHCO}_3 < \text{Na}_2\text{CO}_3 < \text{NaOH}$. It shows that the NaCl increases % adsorption by

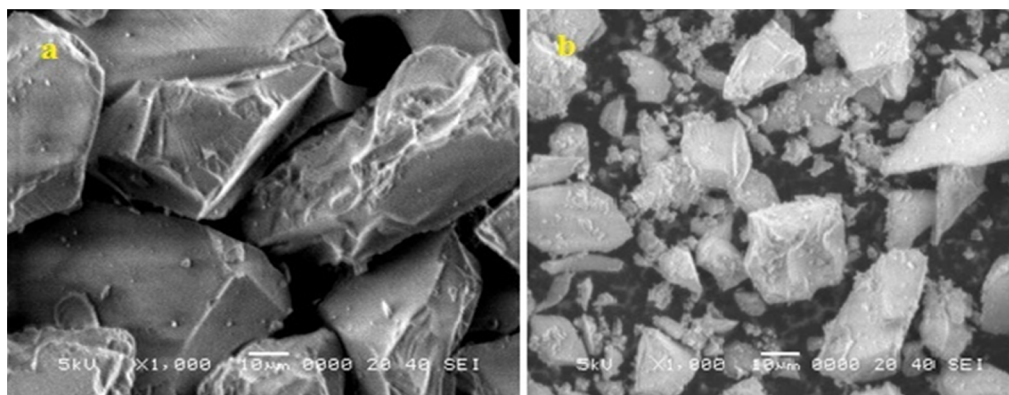


Figure 2. SEM images of (a) pure silica and (b) *p*-piperdinomethylcalix[4]arene-immobilized silica resin PASR.

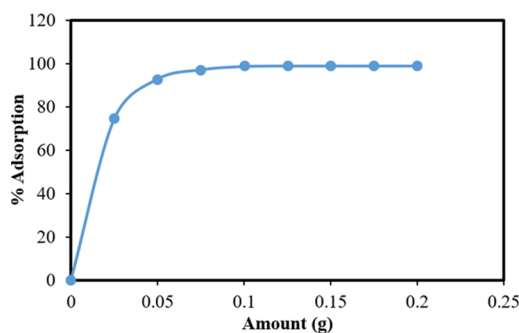


Figure 3. Effect of the adsorbent dosage 0.025–0.2 g on the % adsorption of RB-19 dye (60 min of contact time 0.1 M NaCl and 10 mL of dye concentration 2×10^{-5} M).

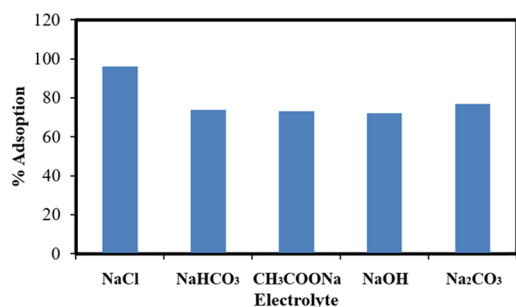


Figure 4. Roles of different electrolytes (concentration: 0.1 M) in the adsorption of RB-19 dye (concentration: 2×10^{-5} M).

increase salting out itself and neutral behavior. Obviously, other electrolytes can disturb the pH value of dye solution; therefore, % adsorption may decrease.

3.3.3. Effect of pH. The role of pH for the ionization of dye solution is very important due to the nature of functional groups present on the surface of the adsorbent.²⁵ In this experiment, pH of dye solution was maintained in a range of pH 1–11, while the adsorbent dosage was 0.125 g, 1 h contact time, 0.1 M NaCl, and 10 mL dye solution (2×10^{-5} M). The maximum adsorption (96%) was observed at pH 4 (Figure 5). Overall, the acidic pH value remains more favorable for the adsorption of RB-19. At the basic pH value, it was observed that % adsorption of RB-19 decreases. The reason behind this dramatical decrease in % adsorption by increasing the pH value is due to the deprotonation of the adsorbent and dye molecule. It may be due to the protonation of nitrogen functionality that coordinates with negatively charged molecules of RB-19. At

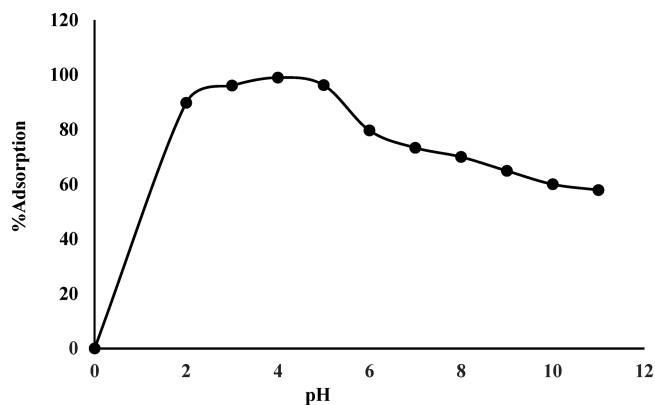


Figure 5. pH effect on the adsorption of RB-19 (0.05 g PASR) 1 h of contact time, 0.1 M NaCl and dye concentration of 2×10^{-5} M.

low pH values, H^+ ions found in surplus that participate with the dye molecule for adsorption sites present over the adsorbent surface. In addition, at higher pH slightly, electrostatic repulsion of negatively charged surface sites does not favor the adsorption of dye molecules onto the adsorbent surface; therefore, % adsorption decreases. It can be clearly observed that the deprotonated amine functionalities of calix[4]arene moiety show less physical interaction toward the ions of RB-19 molecules.

3.4. Adsorption Isotherms. Table 1 shows the parameters calculated from three adsorption isotherms, that is, Langmuir, Freundlich, and Dubinin–Radushkevich (D–R) at different temperatures. Adsorption isotherms explain the mechanism as well as the amount of adsorbate adsorbed onto the surface of the adsorbent.²⁶ The adsorption isotherm also describes the adsorption capacity, multilayer or monolayer formation, and type of interaction in between the adsorbate and adsorbent.^{26–30} Therefore, in this study, Langmuir, Freundlich, and D–R adsorption isotherms have been applied to experimental data under the optimized conditions to assess the adsorption capacity of the adsorbent. The linear forms of these three adsorption isotherms are given as follows:

$$\frac{C_e}{C_{ads}} = \frac{1}{Qb} + \frac{C_e}{Q} \quad (3)$$

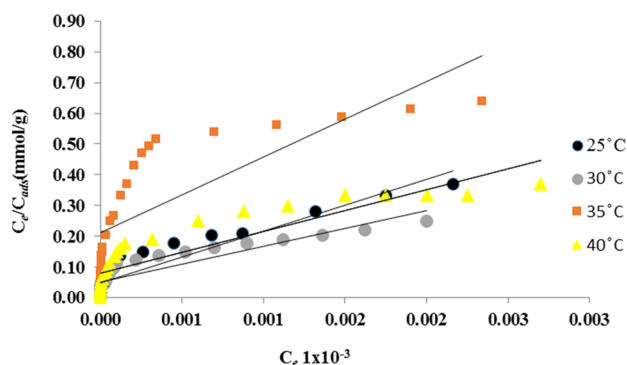
$$\ln C_{ads} = \ln A + \frac{1}{n} \ln C_e \quad (4)$$

$$\ln C_{ads} = \ln X_m - \beta e^2 \quad (5)$$

Table 1. Langmuir, Freundlich, and D–R Adsorption Isotherm Parameters at Different Temperatures

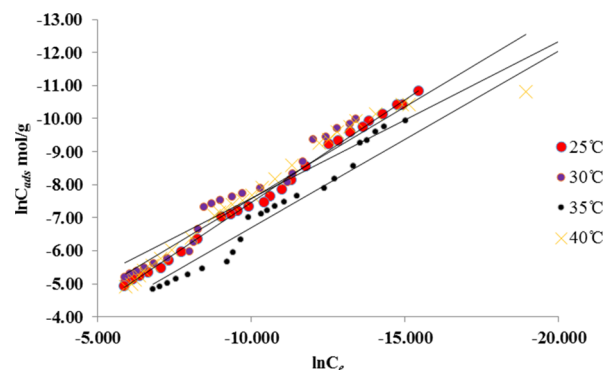
Langmuir				
temperature (K)	Q (mol/g)	b	R _L	R ²
293	3.93	1203	0.99–0.21	0.600
303	5.99	3391	0.99–0.22	0.899
313	8.62	2247	0.99–0.12	0.891
Freundlich				
temperature (K)	A (mg g ⁻¹)	n	R ²	
293	0.0013	2.11	0.838	
303	0.065	1.60	0.99	
313	0.042	1.87	0.99	
D–R				
temperature (K)	X _m (mmol/g)	E (kJ/mol)	R ²	
293	14.17	10.2	0.985	
303	2.70	12.5	0.685	
313	7.09	11.7	0.897	

Langmuir adsorption isotherm is selective and describes that only one molecule or ion can bind to each site of the adsorbent, and there is no interaction in between neighboring ions, increasing the adsorbate concentration, adsorption increases.³¹ The plot of C_e/C_{ads} versus C_e was obtained with a regression coefficient of $R^2 = 0.199$ (Figure 6). However, the adsorption process can be reversible or irreversible and that can be explained by the separation factor R_L ($R_L = 1 + (1/bC_i)$).

**Figure 6.** Langmuir adsorption isotherm plot (concentration: 1.50×10^{-10} to 2.00×10^{-5} M, with 60 min shaking time at different temperatures).

The Freundlich adsorption isotherm model (eq 3) is used to calculate the heterogeneity of the adsorbent surface³² and describes the multilayer adsorption.³³ The graph was plotted for $\ln C_e$ versus $\ln C_{ads}$ (Figure 7). From the slope and intercept, the value of A and n can be calculated. The Freundlich isotherm model shows good regression coefficient R^2 (0.990) suggesting best fit to experimental data for the adsorption of RB-19 dye onto PASR. The value of n reveals the favorability and degree of heterogeneity. Calculated from the Freundlich model, $n > 1$ suggests favorable adsorption conditions.¹⁷

The Dubinin–Radushkevich (D–R) isotherm model is applied to describe and distinguish the physical and chemical adsorption nature of the adsorption mechanism. An important factor in the D–R model, the polynic potential (ϵ) can be calculated as follows:³⁴

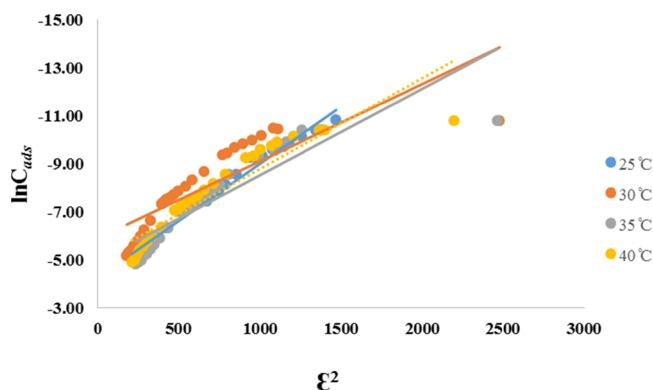
**Figure 7.** Freundlich adsorption isotherm (concentration: 1.50×10^{-10} to 2.00×10^{-5} M, with 60 min shaking time at different temperatures).

$$\epsilon = RT \ln \left(1 + \frac{1}{C_e} \right) \quad (6)$$

In above equation, T shows the absolute temperature (K), whereas R is the ideal gas constant (kJ/mol/K). E shows the mean adsorption energy mentioned below in eq 7:

$$E = \frac{1}{\sqrt{-2\beta}} \quad (7)$$

When the values of ϵ are plotted against $\ln C_{ads}$ (mol/g), a linear graph with a correlation coefficient of $R^2 = 0.977$ was shown in Figure 8. Table 1 shows the results of D–R

**Figure 8.** D–R isotherm (concentration: 1.50×10^{-10} to 2.00×10^{-5} M, with 60 min shaking time at different temperatures).

adsorption models in which the X_m value was found to be 0.343, and the E value 12.9 kJ/mol indicating that the adsorption process is chemical in nature.

3.5. Column Adsorption. The continuous-flow adsorption experiment was conducted in a glass column, and a breakthrough curve was observed against time (Figure 9). The time and shape of the curve were important parameters to analyze the column operation and response of the column adsorption. The position of the curve depends upon the flow rate and concentration of dye solution. The breakthrough curve can be describe in terms of the inlet dye concentration (C_i), concentration of dye adsorbed (C_s), and outlet concentration of dye (C_t) or normalized concentration. It can be defined as the ratio of the effluent concentration of dye-to-inlet concentration of dye (C_t/C_o) as a function of volume of the effluent or time. The optimized conditions for the batch

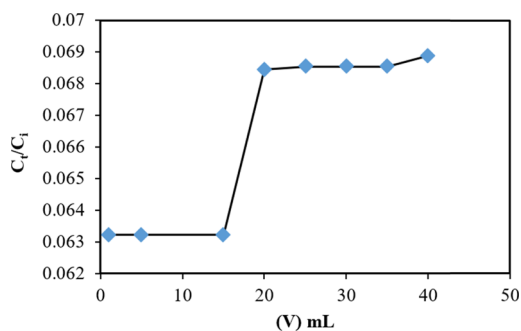


Figure 9. Breakthrough curve of RB-19 dye (concentration: 2.00×10^{-5} M).

adsorption study were also applied in the dynamic adsorption at a flow rate of 2 mL min^{-1} to remove RB-19 (2×10^{-5} M) from water through PASR (0.125 g). The breakthrough volume was calculated from the plot of C_t/C_i versus V (mL). The results show that the column achieved breakthrough at $C_t/C_i = 0.21$ RB-19 dye with a bed volume of 5 mL and took approximately 25 mL to exhaust.

3.5.1. Thomas Model. The knowledge of the breakthrough curve or concentration time profile helps to design the column, which should be effective and have the maximum removal capacity of target molecules. Usually, the Thomas model is an effective tool to evaluate the results of the column adsorption. The results of dynamic adsorption data were analyzed through the Thomas model to determine (q_0), which is the maximum solid-phase concentration and the (k_{TH}) Thomas rate constant. Equation 8 shows the linear form Thomas model, and constants values were calculated by plotting the graph for $\ln\left(\frac{C_i}{C_e} - 1\right)$ against t (min) at the constant flow rate (figure 10). The magnitude of the maximum solid phase concentration

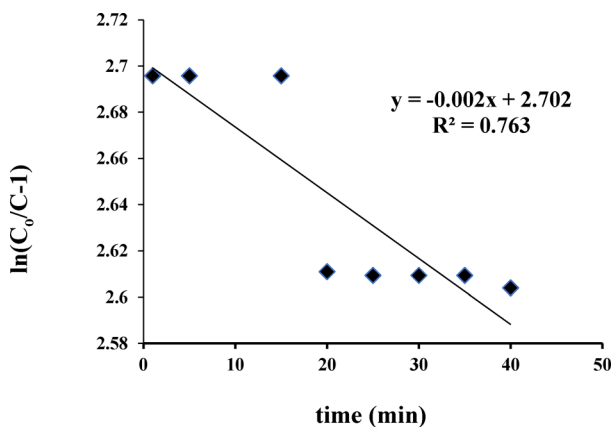


Figure 10. Thomas model graph of $\ln\left(\frac{C_i}{C_e} - 1\right)$ vs t for RB-19 dye (concentration: 2.00×10^{-5} M).

of the solute and Thomas model rate constant k_{TH} was found to be 2.702 with the coefficient of determination ($R^2 = 0.76$) for RB-19.

$$\left(\ln \frac{C_i}{C_e} - 1\right) = \frac{k_{TH} q_0 A}{Q} - \frac{k_{TH} C_i V_{\text{eff}}}{Q} \quad (8)$$

Here, C_i and C_e show the initial concentration and effluent concentration (mg L^{-1}), respectively. Q is the flow rate

(mL min^{-1}), A is the quantity of material adsorbed, and V_{eff} expresses the effluent volume, which can be obtained from the q 9

$$V_{\text{eff}} = Q t_{\text{total}} \quad (9)$$

where t_{total} stands for the total flow time, Q is the flow rate, and V_{eff} stands for the effluent volume.

3.5.2. Kinetic Study. Kinetics is an important factor for the determination of the adsorption mechanism. Experimental data was fitted to two well-known kinetic models, namely, Langergren or pseudo-first-order (q 10) that is based on assumption that the rate-limiting step may be the physical adsorption, whereas Ho and McKay or the pseudo-second-order kinetic (q 11) model suggest that the adsorption mechanism is the rate-controlling step and chemical in nature^{35,36}

$$\ln(q_e - q_t) = \ln q_e - k_1 t \quad (10)$$

$$\frac{t}{q_t} = \left(\frac{1}{k_2 q_e^2}\right) + \left(\frac{1}{q_e}\right) t \quad (11)$$

where k_1 and k_2 are the adsorption rate constants for pseudo-first-order and pseudo-second-order kinetics, respectively. The linear relationship was observed for the pseudo-first-order kinetic and pseudo-second-order kinetic models as shown in Figures 11 and 12. The values of k_1 , k_2 (1/min), and q_e (mg/g)

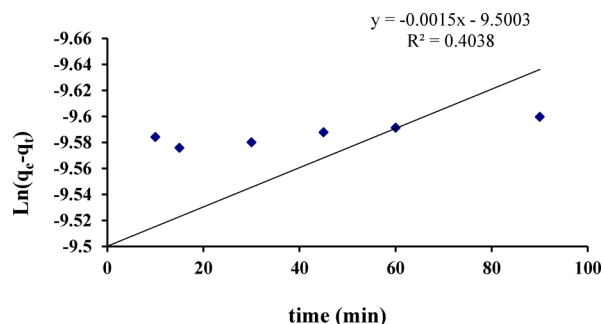


Figure 11. Pseudo-first-order kinetic graph for RB-19 dye (60 min of contact time, 0.1 M NaCl, and 10 mL of dye with a concentration of 2×10^{-5} M).

were obtained from the slopes and intercepts of the linear plots and presented in Table 2. Parameters in Table 2 show that the

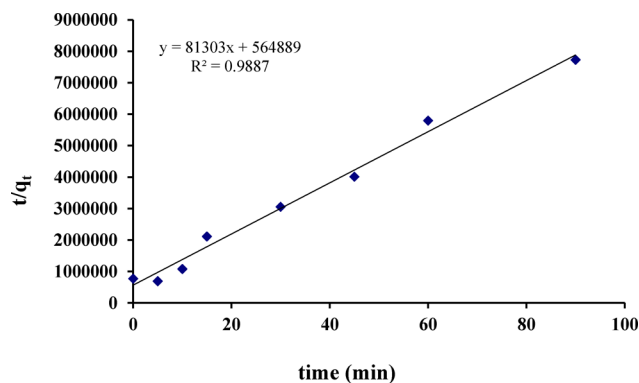


Figure 12. Pseudo-second-order graph (60 min of contact time, 0.1 M NaCl, and 10 mL of dye with a concentration of 2×10^{-5} M).

Table 2. Comparison of Kinetic Models

temperature	pseudo-first-order kinetic model			pseudo-second-order kinetic model		
	K_1 (1/min)	q_e (mol/g)	R^2	K_2 (g/mol/min)	q_e (mol/g)	R^2
303	0.0001	0.0700	0.589	16276.3	2.12×10^{-07}	0.972
308	0.0010	0.0700	0.297	30185.8	3.43×10^{-07}	0.999
313	0.0379	0.0237	0.872	8138.7	8.20×10^{-06}	0.999

kinetic mechanism follows the pseudo-second-order model as experimental data significantly fitted well with the correlation coefficient value of $R^2 = 0.99$,

3.5.3. *Thermodynamics of Adsorption.* Different thermodynamic factors concerning the adsorption method, for example, ΔH (kJ/mol), ΔS (J/mol/K), and ΔG (kJ/mol) were estimated from following equations

$$\ln K_C = \frac{-\Delta H}{RT} + \frac{\Delta S}{R} \quad (12)$$

$$\Delta G = -RT \ln K_C \quad (13)$$

where ΔH is enthalpy, ΔS is entropy, ΔG is the Gibbs free energy, and T is the absolute temperature, R is the gas constant, and K_C is the equilibrium constant. The temperature effect was observed in the range of 293 to 313 K on the adsorption of RB-19 on PASR under optimum conditions. It has been observed that increasing the temperature ultimately increases the adsorption capacity (Figure 13).

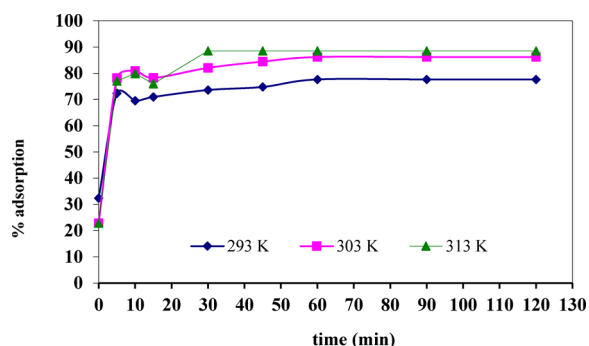


Figure 13. % adsorption curves of RB-19 onto PASR as a function of different temperatures from 293 to 313 K.

The mathematical values of ΔH and ΔS were calculated from the plot of $\ln K_C$ versus $1/T$ using eq 12 (Figure 14) and presented in Table 3.

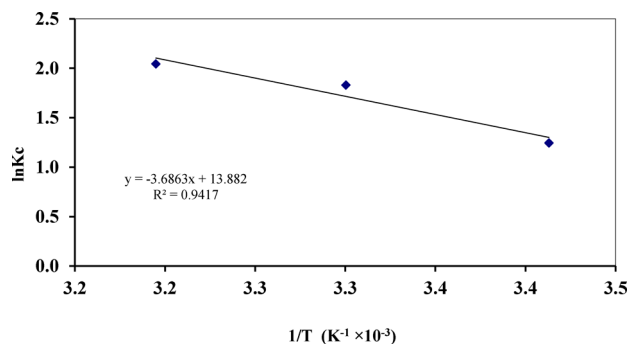


Figure 14. Effect of the temperature on the adsorption of the RB-19 azo dye onto *p*-piperdinomethylcalix[4]arene-immobilized silica resin (PASR).

Table 3. Thermodynamic Parameters for RB-19 onto the PASR

ΔH (kJ/mol)	ΔS (kJ/mol/K)	ΔG (kJ/mol)		
		303 K	308 K	313 K
-0.03	0.115	-3.03	-4.61	-5.32
		$\ln K_C = 1.2$	$\ln K_C = 1.8$	$\ln K_C = 2.0$

The negative value of ΔG under applied conditions implies the spontaneity of the dye adsorption process. Moreover, the exothermic nature of adsorption observed from the negative value of ΔH . Additionally, the increase in the value of $\ln K_C$ (1.2, 1.8, and 2.0 at 303, 308, and 313 K, respectively) with the rise of temperature showed that the RB-19 adsorption onto PASR was an exothermic process and does not depend on the temperature. The randomness increases during the adsorption at the solid/solution, an edge that implies its positive value.

3.5.4. *Field Application of PASR.* To ensure the PASR as a competent adsorbent for RB-19, a field study of PASR for real wastewater samples containing RB-19 dye has also been carried out. Batch experiments have been performed with PASR contaminated with RB-19 at the optimized conditions. The concentration of RB-19 dye was investigated before and after the treatment of wastewater samples by UV–VIS spectrophotometry at its particular wavelength 593 nm. The results are summarized in Table 4. The lower concentration of RB-19 in

Table 4. RB-19 Dye Concentration in the Wastewater Samples before and after Treatment with the PASR

sample no.	concentration before treatment (ppm)	concentration after treatment (ppm)	% removal
1	0.836	0.0157	98.12
2	0.750	0.2306	69.26
3	0.552	0.0403	92.69

the wastewater samples after the treatment indicates that PASR is an efficient adsorbent and could be successfully employed for the decontamination of RB-19 from the industrial effluent. A comparative table (Table 5) has been provided to show the efficiency of PASR with other synthesized material. It can be observed that PASR has good efficiency along with other reported materials.

4. CONCLUSIONS

In summary, the work demonstrates the synthesis of *p*-piperdinomethylcalix[4]arene-immobilized silica resin (PASR) and its application for the removal of RB-19 from the industrial effluent. Experimental results show that the adsorption of RB-19 is pH dependent, and the adsorption process follows the Freundlich and Dubinin–Radushkevich (D–R) isotherm models. Thermodynamic and kinetic studies suggest that the adsorption process is exothermic and spontaneous in nature and follow the pseudo-second-order kinetic model. Moreover,

Table 5. Comparison of PASR with Other Adsorbents for the Removal of Azo Dyes

adsorbent	azo dye	pH	% adsorption	ref
laccase-immobilized silica	acid orange 7	4–6	31	37
horseradish peroxidase	acid orange 7	5.0	89	38
horseradish peroxidase (HRP)-immobilized calcium alginate gel beads	acid orange 7	7.4	75	39
Fe ₃ O ₄ @L-arginine nanoparticles	RB-19	3.0	96	40
nanofiber mats	RB-19	1.0	98	17
PASR	RB-19	4.0	96	present study

the field studies of real water samples also supported the PASR as an effective adsorbent for the decontamination of RB-19 dye.

AUTHOR INFORMATION

Corresponding Author

*E-mail: ayazmemon33@gmail.com. Phone: +92 (22) 9213430. Fax: +92 (22) 9213431.

ORCID

Ayaz Ali Memon: 0000-0002-9018-4856

Notes

The authors declare no competing financial interest.

ACKNOWLEDGMENTS

We are highly thankful to the National Centre of Excellence in Analytical Chemistry, University of Sindh, Jamshoro, Sindh, Pakistan for the financial support of this work.

REFERENCES

- Chung, K.-T. Azo dyes and human health: a review. *J. Environ. Sci. Health, Part C: Environ. Carcinog. Ecotoxicol. Rev.* **2016**, *34*, 233–261.
- Balakrishnan, V. K.; Shirin, S.; Aman, A. M.; de Solla, S. R.; Mathieu-Denoncourt, J.; Langlois, V. S. Genotoxic and carcinogenic products arising from reductive transformations of the azo dye, Disperse Yellow 7. *Chemosphere* **2016**, *146*, 206–215.
- Harichandran, G.; Prasad, S. SonoFenton degradation of an azo dye, Direct Red. *Ultrason. Sonochem.* **2016**, *29*, 178–185.
- Marim, R. A.; Oliveira, A. C. C.; Marquezoni, R. S.; Servantes, J. P. R.; Cardoso, B. K.; Linde, G. A.; Colauto, N. B.; Valle, J. S. Use of sugarcane molasses by *Pycnoporus sanguineus* for the production of laccase for dye decolorization. *Genet. Mol. Res.* **2016**, *15*, gmr15048972.
- Mojsov, K. D.; Andronikov, D.; Janevski, A.; Kuzelov, A.; Gaber, S. The application of enzymes for the removal of dyes from textile effluents. *Adv. Technol.* **2016**, *5*, 81–86.
- Yilmaz Ozmen, E.; Erdemir, S.; Yilmaz, M.; Bahadir, M. Removal of carcinogenic direct azo dyes from aqueous solutions using calix [n] arene derivatives. *Clean: Soil, Air, Water* **2007**, *35*, 612–616.
- Lalnunhlimi, S.; Krishnaswamy, V. Decolorization of azo dyes (Direct Blue 151 and Direct Red 31) by moderately alkaliphilic bacterial consortium. *raz. J. Microbiol.* **2016**, *47*, 39–46.
- Qureshi, U. A.; Khatri, Z.; Ahmed, F.; Khatri, M.; Kim, I.-S. Electrospun zein nanofiber as a green and recyclable adsorbent for the removal of reactive black 5 from the aqueous phase. *ACS Sustainable Chem. Eng.* **2017**, *5*, 4340–4351.
- Giannakoudakis, D. A.; Kyzas, G. Z.; Avranas, A.; Lazaridis, N. K. Multi-parametric adsorption effects of the reactive dye removal with commercial activated carbons. *J. Mol. Liq.* **2016**, *213*, 381–389.

(10) Li, C.; Xiong, Z.; Zhang, J.; Wu, C. The strengthening role of the amino group in metal–organic framework MIL-53 (Al) for methylene blue and malachite green dye adsorption. *J. Chem. Eng. Data* **2015**, *60*, 3414–3422.

(11) Öztürk, A.; Abdullah, M. I. Toxicological effect of indole and its azo dye derivatives on some microorganisms under aerobic conditions. *Sci. Total Environ.* **2006**, *358*, 137–142.

(12) Rawat, D.; Mishra, V.; Sharma, R. S. Detoxification of azo dyes in the context of environmental processes. *Chemosphere* **2016**, *155*, 591–605.

(13) Kant, R. Textile dyeing industry an environmental hazard. *Nat. Sci.* **2012**, *4*, 22–26.

(14) Gupta, V. K. Application of low-cost adsorbents for dye removal—a review. *J. Environ. Manage.* **2009**, *90*, 2313–2342.

(15) Crini, G. Non-conventional low-cost adsorbents for dye removal: a review. *Bioresour. Technol.* **2006**, *97*, 1061–1085.

(16) Garg, V. K.; Amita, M.; Kumar, R.; Gupta, R. Basic dye (methylene blue) removal from simulated wastewater by adsorption using Indian Rosewood sawdust: a timber industry waste. *Dyes Pigm.* **2004**, *63*, 243–250.

(17) Hakro, R. A.; Qureshi, U. A.; Qureshi, R. F.; Mahar, R. B.; Khatri, M.; Ahmed, F.; Khatri, Z.; Kim, I. S. Efficient Removal of Reactive Blue 19 Dye by Co-Electrospun Nanofibers. *Preprints* **2018**, DOI: 10.20944/preprints201807.0108.v1.

(18) Shinkai, S. Functionalized Calixarenes: New Applications as Catalysts, Ligands, and Host Molecules. In *Calixarenes: A Versatile Class of Macrocyclic Compounds*; Springer: 1991, 173–198.

(19) Joseph, R.; Rao, C. P. Ion and molecular recognition by lower rim 1, 3-di-conjugates of calix [4] arene as receptors. *Chem. Rev.* **2011**, *111*, 4658–4702.

(20) Israr, M.; Faheem, F.; Minhas, F. T.; Rauf, A.; Rauf, S.; Shah, M. R.; Rahim, F.; Shah, K.; Bhangar, M. I. Extraction Properties of Calix [4] arenes towards Sulphonated Dyes. *Am. J. Anal. Chem.* **2016**, *7*, 219.

(21) Gutsche, C. D.; Iqbal, M.; Stewart, D. Calixarenes. 19. Syntheses procedures for p-tert-butylcalix [4] arene. *J. Org. Chem.* **1986**, *51*, 742–745.

(22) Gutsche, C. D.; Levine, J. A. Calixarenes. 6. Synthesis of a functionalizable calix [4] arene in a conformationally rigid cone conformation. *J. Am. Chem. Soc.* **1982**, *104*, 2652–2653.

(23) Gutsche, C. D.; Nam, K. C. Calixarenes. 22. Synthesis, properties, and metal complexation of aminocalixarenes. *J. Am. Chem. Soc.* **1988**, *110*, 6153–6162.

(24) Jal, P. K.; Patel, S.; Mishra, B. K. Chemical modification of silica surface by immobilization of functional groups for extractive concentration of metal ions. *Talanta* **2004**, *62*, 1005–1028.

(25) Errais, E.; Duplay, J.; Darragi, F.; M'Rabet, I.; Aubert, A.; Huber, F.; Morvan, G. Efficient anionic dye adsorption on natural untreated clay: Kinetic study and thermodynamic parameters. *Desalination* **2011**, *275*, 74–81.

(26) Dąbrowski, A. Adsorption—from theory to practice. *Adv. Colloid Interface Sci.* **2001**, *93*, 135–224.

(27) McCash, E. M. *Surface chemistry*; Oxford University Press: United Kingdom, 2001.

(28) Helfferich, F. G. *Ion Exchange*; McGraw-Hill: 1962.

(29) Itodo, A. U.; Itodo, H. U. Utilizing D-R and Temkin isotherms with GCMS external standard technique in forecasting liquid phase herbicide sorption energies. *Electron. J. Environ., Agric. Food Chem.* **2010**, *9*, 1792–1802.

(30) McKay, G.; Blair, H. S.; Gardner, J. R. Adsorption of dyes on chitin. I. Equilibrium studies. *J. Appl. Polym. Sci.* **1982**, *27*, 3043–3057.

(31) Langmuir, I. The adsorption of gases on plane surfaces of glass, mica and platinum. *J. Am. Chem. Soc.* **1918**, *40*, 1361–1403.

(32) Appel, J. Freundlich's adsorption isotherm. *Surf. Sci.* **1973**, *39*, 237–244.

(33) Bhatti, A. A.; Kamboh, M. A.; Solangi, I. B.; Memon, S. Synthesis of calix [6] arene based XAD-4 material for the removal of

reactive blue 19 from aqueous environments. *J. Appl. Polym. Sci.* **2013**, *130*, 776–785.

(34) Polanyi, M. Section III.—theories of the adsorption of gases. A general survey and some additional remarks. Introductory paper to section III. *Trans. Faraday Soc.* **1932**, *28*, 316–333.

(35) Ho, Y.-S. Second-order kinetic model for the sorption of cadmium onto tree fern: a comparison of linear and non-linear methods. *Water Res.* **2006**, *40*, 119–125.

(36) Ho, Y. S.; McKay, G. Sorption of dye from aqueous solution by peat. *Chem. Eng. J.* **1998**, *70*, 115–124.

(37) Akceylan, E.; Bahadir, M.; Yilmaz, M. Removal efficiency of a calix[4]arene-based polymer for water-soluble carcinogenic direct azo dyes and aromatic amines. *J. Hazard. Mater.* **2009**, *162*, 960–966.

(38) Yilmaz, E.; Memon, S.; Yilmaz, M. Removal of direct azo dyes and aromatic amines from aqueous solutions using two β -cyclodextrin-based polymers. *J. Hazard. Mater.* **2010**, *174*, 592–597.

(39) Gholami-Borujeni, F.; Mahvi, A. H.; Naseri, S.; Faramarzi, M. A.; Nabizadeh, R.; Alimohammadi, M. Application of immobilized horseradish peroxidase for removal and detoxification of azo dye from aqueous solution. *Res. J. Chem. Environ.* **2011**, *15*, 217–222.

(40) Dalvand, A.; Nabizadeh, R.; Ganjali, M. R.; Khoobi, M.; Nazmara, S.; Mahvi, A. H. Modeling of Reactive Blue 19 azo dye removal from colored textile wastewater using L-arginine-functionalized Fe_3O_4 nanoparticles: Optimization, reusability, kinetic and equilibrium studies. *J. Magn. Mater.* **2016**, *404*, 179–189.